Available online at www.sciencedirect.com
SCIENCE DIRECT®
ELSEVIER
Ultramicroscopy 101 (2004) 231–240
ultramicroscopy
www.elsevier.com/locate/ultramic

Tip to substrate distances in STM imaging of biomolecules

Dario Alliata, Laura Andolfi, Salvatore Cannistraro*

Biophysics & Nanoscience Centre, INFM, Dipartimento di Scienze Ambientali, Università della Tuscia, I-01100 Viterbo, Italy

Received 25 November 2003; received in revised form 3 June 2004; accepted 21 June 2004

Abstract

STM images of single biomolecules adsorbed on conductive substrates do not reproduce the expected physical height, which generally appears underestimated. This may cause the tip to interfere with the soft biological sample during the imaging scans. Therefore, a key requirement to avoid invasive STM imaging is the knowledge, and the control, of the initial tip to substrate distance. This is connected to the setting of the tunnelling current and applied voltage, which define a tunnelling resistance.

The height of the STM tip was measured by calibrating the tunnelling resistance, as a function of its vertical displacement until establishing a mechanical contact. At a tunnelling resistance of $4 \times 10^9\,\Omega$, distances of about 3 and 6 nm are estimated when flat Au substrates are imaged in water and in air, respectively. On such a ground, the relevance of the starting tip–substrate distance in determining a non-invasive imaging has been investigated for a plastocyanin mutant chemisorbed on Au(1 1 1) electrodes. At tunnelling distances sufficient to overcome the physical height of the imaged biomolecules, their lateral dimensions are found to be consistent with the crystallography, whereas they are significantly broadened for smaller distances.

PACS: 87.64.Dz; 87.14.Ee

Keywords: Scanning tunnelling microscopy; Tunnelling distances; Copper protein; Plastocyanin mutant

1. Introduction

Since its introduction, STM has been exploited to investigate a large number of biomolecules like proteins and DNA immobilized on conductive substrates [1–3].

The discovery that STM could be operated under fluid [4] opened the feasibility of high-resolution studies of biomolecules in a near-physiological condition [5]. The introduction of the electrochemical control [6] extended the potentiality of in situ STM to study the heterogeneous electron transfer mechanism between

*Corresponding author. Tel.: +39-0761-357136; fax: +39-0761-357136/179.
E-mail address: cannistr@unitus.it (S. Cannistraro).

0304-3991/$ - see front matter © 2004 Elsevier B.V. All rights reserved.
doi:10.1016/j.ultramic.2004.06.005

redox biomolecules and metal electrodes, whose knowledge is crucial for the development of bioelectronic devices [7–9].

Several groups have reported successful STM imaging of biomolecules in various environments [10–21]; nevertheless, the mechanism governing the tunnelling current through the biological material, due also to the large complexity of the biological macromolecular structure, has not been fully elucidated.

Irrespective of the electron conduction mechanism, the height of biomolecules as estimated by STM is found significantly lower as compared with the crystallographic data [12,19,20,22–25]. This may be connected to both the poor conductive properties of the biological matter and the electric resistance present at the molecule–electrode junction [26–28]. When STM is operated in constant current mode, the estimated height of a single molecule on a flat metal surface corresponds to the vertical tip retraction as governed by the feedback loop, which compensates the piezo position for a variation in current reading. As a major consequence, the scans will perturb the macromolecular structure if the tip retraction is not sufficient to overcome the top of the biomolecule. On the other hand, an unperturbed imaging of biomolecules is fundamental to discriminate between intrinsic conductive properties and tip-induced effects, especially in the attempt to model the tunnelling mechanism through a biomolecule [29–33]. For example, if the tip penetrates the biomolecule, it is difficult to know which part has contributed to the current.

In general, the absolute vertical position of the tip over the conductive substrate is difficult to be estimated. Therefore, the tip–sample distance can be inferred from the tunnelling current and bias voltage settings, once the corresponding resistance has been calibrated as function of the tunnelling gap width and a reliable contact resistance value has been assumed [34,35].

The transition from tunnelling to contact regime was firstly studied in ultra-high vacuum junctions [36,37]. The current shows an exponential dependence on distance consistent with a rectangular tunnelling barrier model [38]; the measured contact resistance (about $10^4\,\Omega$) having been found very close to the theoretical prediction of Lang [39].

Bingelli et al. [40] extended the investigation of the point contact regime to water electrolytes. Controlled variation of the tip–sample distance in the transition regime exhibited a similar distance dependence of the tip current as observed in previous vacuum studies. In this electrolytic system, a distance variation of 1 nm was registered if the tunnelling resistance was reduced from 10^7 to $10^4\,\Omega$. At similar conclusions arrived Vaught et al. [34], who estimated a tunnel gap of 2 nm at $10^9\,\Omega$ for an Au(1 1 1) substrate imaged under electrolyte. As predicted by the dielectric model [41], the increase in tunnelling distances under electrolyte, was explained by a lowering of the apparent tunnelling barrier height as due to the presence of water [42–44].

For STM imaging performed in ambient atmosphere, larger tunnelling distances were found. At a resistance of $10^8\,\Omega$, a corresponding tunnelling gap of 3 nm was measured on hydrophilic surfaces [45], while up to 10 nm gaps were estimated during imaging of bacteriophage tails on indium oxide [46].

In summary, the significant scattering of data in literature points out that the distance–resistance dependence is strongly influenced by the medium in which the measurements are performed.

In this work, the width of the tunnelling gap between the scanning tip and the gold substrate has been determined, and its relevance for a non-invasive imaging has been investigated for a poplar plastocyanin variant protein immobilized on Au(1 1 1).

Poplar plastocyanin is a small (10.5 KDa) copper protein which functions as an electron carrier in the photosynthetic chain. The protein has an 8-stranded antiparallel beta sheet structure and a redox (CuII–CuI) copper active site located at the northern part of the protein. This site is coordinated by four amino acid residues in a tetrahedral geometry which provides the protein with its peculiar spectroscopic and electrochemical features [47]. Site directed mutagenesis has been used to introduce a disulfide group in the protein (PCSS) sequence opposite to the redox site in order to obtain a stable chemical link with gold substrates [48].

From the dependence of the tunnelling resistance on the vertical tip position, we inferred tunnelling distances of about 3 and 6 nm in water and in air, respectively, at a working resistance of $4 \times 10^9\,\Omega$.

The effect of a controlled variation of the tip–substrate distance on the imaging of the biomolecules placed in the tunnelling gap allowed us to indicate optimal conditions for non-invasive STM of biomolecules.

2. Experimental details

Design and expression of PCSS has been described in detail elsewhere [48]. Briefly, the pET-3a plasmid, which contains the poplar plastocyanin gene was used as template and the mutation was incorporated with a mutagenic primer carrying the mutated codons. The expression vector, containing the mutated gene, was reconstructed by a combination of restriction sites. The mutant protein was overexpressed in the cytoplasma of *E.coli* cells and released from the bacterial cells by freeze-thaw method. PCSS was purified by anion exchange chromatography (DEAE Sepharose-fast flow) and size exclusion column (Superdex G-75) in a Pharmacia FPLC set-up. The protein purity was assessed by SDS page and isoelectric focusing gel (PhastGel IEF 3-9 Pharmacia).

STM experiments were performed either in ambient atmosphere or in ultra-pure water (18.2 MΩ cm) with a PicoScan STM instrument (Molecular Imaging, Inc.) equipped with a 10 μm scanner and a preamplifier sensitivity of 1 nA/V, which records a maximum current of 10 nA and applies minimum voltage bias of 10 mV. Fluid STM experiments were carried out by using a Teflon liquid cell.

STM tips were prepared either by electrochemical etching of Pt/Ir wire (Goodfellow) and coated with apiezon wax or mechanically from Pt/Ir wire. Substrates consisted of Au films thermally evaporated on borosilicate (Arrandee™) and butane flame annealed to reconstruct (1 1 1) terraces.

Recrystallized gold substrates were incubated with 50 μM of PCSS solution in 20 mM sodium phosphate (pH 6) between 40 min and 1 h at 4° C.

Mono disperse gold colloids with nominal diameter of 5 nm (Sigma Aldrich, Co.) were deposited on Au(1 1 1) at a concentration of 3×10^{-8} M and left to dry overnight in drying box filled with silica gel. The height of colloids on Au terraces was controlled by Tapping Mode AFM (TMAFM) performed with a Nanoscope IIIA system (Digital Instruments).

Current vs. distance measurements were obtained by positioning the STM tip on a flat Au(1 1 1) terrace, at starting tunnelling resistance in the range between 2×10^8 and $2 \times 10^{10}\,\Omega$. The current was recorded as function of vertical distance during approach or withdraw of the STM tip, in a time scale between 0.1 and 0.3 s. Data were processed if vertical thermal drift of piezo actuator relative to the substrate was below 0.05 nm/s. When the tunnelling current, I_T, resulted to be proportional to $\exp(-ks)$, the inverse decay length $k = -1/2(\mathrm{d}\ln I_T/\mathrm{d}s)$ was evaluated by fitting $\ln I_T$ as a function of the vertical tip position s.

STM images were performed at several scan speeds; with no significant changes in the overall features having been observed in the range of 2–4 Hz. Moreover, STM imaging was independent of scan direction.

3. Results and discussion

Tunnelling current I_T, is expected to vary with the tunnelling gap, s, proportionally to $\exp(-ks)$, where k is the inverse decay length that is equal to $-1/2(\mathrm{d}\ln I_T/\mathrm{d}s)$.

To investigate any possible influence of tunnelling parameters (current, bias) on k, the dependence of the tunnelling current on the tip–substrate distance was measured on flat Au(1 1 1) in ambient atmosphere at starting tunnelling resistances ranging between 2×10^8 and $2 \times 10^{10}\,\Omega$ typical result is shown in Fig. 1, where the logarithm of current is displayed as a function of the vertical tip displacement, which is controlled by the piezo actuator. The dependence

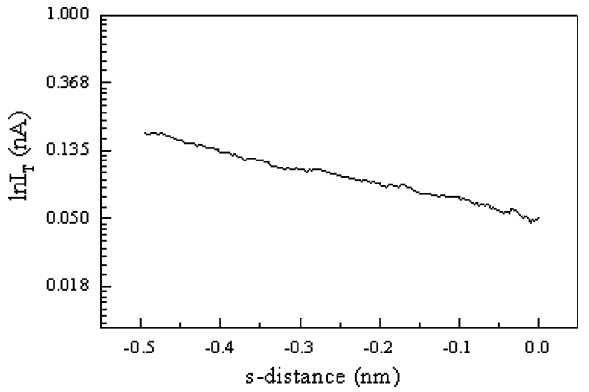

Fig. 1. Tunnelling current vs. vertical tip position for a Pt–Ir tip and an Au(1 1 1) substrate, as recorded at a constant bias of 0.02 V. The zero point in the *s*-horizontal axis refers to the starting piezo position, which is unknown and corresponds to a tunnelling resistance of $2\times10^8\,\Omega$; negative value for *s* means that the tip is moving towards the substrate.

of the current on the distance appears strictly exponential and the *k* value, as calculated from the slope of $\ln I_T$, results to be almost constant and, therefore, not affected by the starting tunnelling conditions.

We focused, then, the attention on the current–distance characteristics of the tunnelling junction at experimental conditions generally used to image proteins [25,31]. We engaged in feedback at unknown absolute height, but at a tunnelling resistance of $4\times10^9\,\Omega$ (50 pA, 0.2 V), we step in d*s* and measured changes in current.

This was repeated for several combinations of gold substrates and Pt–Ir tips, either in air or in ultra-pure water at room temperature. All data recorded are summarized in Table 1. Although, as already observed [40], the calculated values of *k* scatter considerably, they lower in air than in water. This means that the current decays with the tip–substrate distance more rapidly if the measure is performed in ultra-pure water. Moreover, a slight but systematic bias polarity effect is also observable in both media, in agreement with what was suggested previously [34,35].

The absolute tip–substrate distance can be estimated from both measuring the current dependence on vertical tip displacement and the assumption of a reliable value for the electric resistance at the contact point [34,35]. Fig. 2(a)

Table 1
Measurements of $k=-1/2(\mathrm{d}\ln I_T/\mathrm{d}s)$ for different Pt–Ir tips and Au substrates as recorded at a tunnelling resistance of $4\times10^9\,\Omega$

Environment	V_{Bias}	k (nm^{-1})
Air	Positive	1.43 ± 0.46
Air	Negative	1.39 ± 0.54
Water	Positive	3.04 ± 0.97
Water	Negative	2.30 ± 0.81

Data have been collected in air and in ultrapure water with either positive or negative applied bias. The errors correspond to 1-sigma standard deviation.

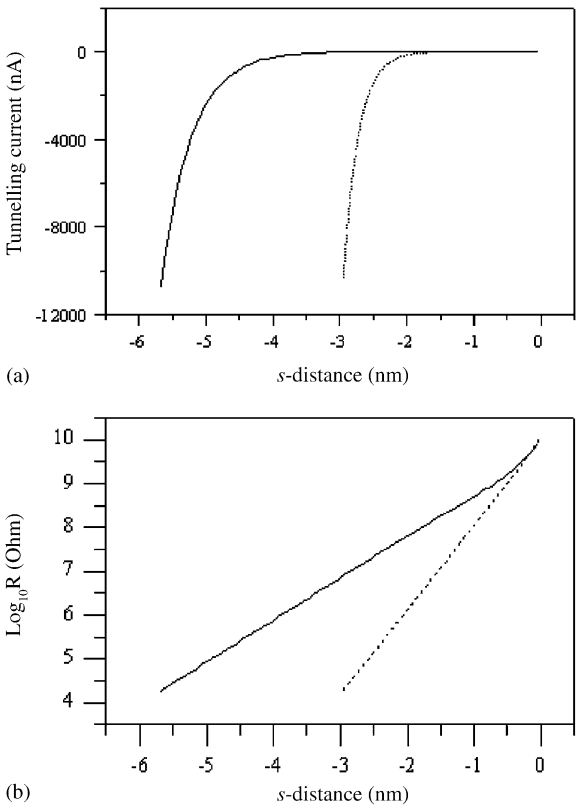

Fig. 2. (a) Fit of I_T vs. distance *s* as recorded during tracing of the tip toward the sample in air (plane line) and in ultra-pure water (dot line), and extrapolated to the current value at contact, having assumed a contact resistance of $2\times10^4\,\Omega$. Zero position refers a tunnelling resistance of $4\times10^9\,\Omega$ (50 pA, 0.2 V). (b) Log (base 10) of the tunnelling resistance plotted against the vertical tip position.

shows the fit of the experimental current values recorded both in air and in ultra-pure water as function of s. The data are extrapolated to the current value corresponding to the contact resistance ($I = V/R_{\text{contact}}$) where for R_{contact} a value of $2 \times 10^4\,\Omega$ has been assumed. Such value is reasonably consistent with our experimental conditions (tip and substrate materials) as reported in literature [36–40]. The exponential increase of the tunnelling current on reducing the distance, is much faster if both substrate and tip are under water. At a fixed bias, the tunnelling current is inversely proportional to the resistance, therefore from Fig. 2(a) a more useful resistance–distance curve can be drawn (Fig. 2(b)). It can be seen that the distance between the initial tip position (at a resistance of $4 \times 10^9\,\Omega$ and the contact position (at resistance of $2 \times 10^4\,\Omega$) is found to be about 3 and 6 nm in water and air, respectively. These values are in good agreement with the results reported previously in the two environments [34,35].

Despite being fast and non-destructive, the estimation of the tunnelling distance from the corresponding resistance is potentially subject to some sources of errors. For instance, positions to establish electrical or mechanical contacts may slightly differ [49]; moreover, the inverse decay length may change within the full path travelled by the tip.

To get an independent estimate of the tunnelling distance, we approached, in a controlled way, the tip to the gold substrate until a mechanical contact was achieved. Simultaneous STM imaging could provide evidence for possible changes in the surface features. For this purpose, STM was set to operate in water at $4 \times 10^9\,\Omega$ (50 pA, 0.2 V) and from the corresponding resistance–distance curve a tunnelling gap of 2.9 nm was estimated. Hence, the tip was approached to the substrate by stepping in ds by 0.1 nm. After 3 nm of tip lowering, the presence of a bump (about 2 nm in height and 10 nm in width) was detected (Fig. 3). Due probably to some damage occurring to the tip the imaging resolution sometimes was not good; however, it was sufficient to witness the occurrence of a mechanical impact, as already reported [50,51]. Various tip–substrate approach experiments were repeated at different starting tunnelling resistances, either in water or in air. Bump dimensions were changed from experiment to experiment, but no systematic effect of the environment or tunnelling resistance was observed. Furthermore, the polarity of the bias applied did not show any influence on the formation of the bump.

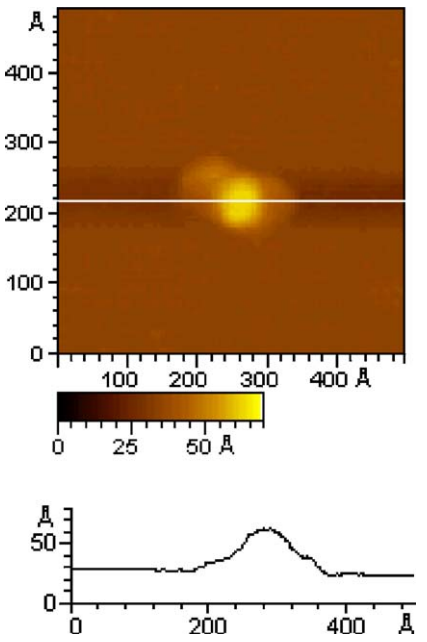

Fig. 3. Constant current STM image of an Au(1 1 1) substrate in ultra-pure water at a tunnelling resistance of $4 \times 10^9\,\Omega$, after having established a mechanical contact with the substrate. Height profile along horizontal white line is shown below.

In conclusion, bumps are generated after the tip has covered a distance that is very close to that we inferred by the resistance–distance characteristics and this confirms that our assumptions were reasonable.

Once tunnelling distances were quantified, we investigated the effect of variations of the tunnelling distance on the intrusiveness of the STM measurements on biomolecules.

Two kinds of samples were imaged: gold colloids and plastocyanin mutant proteins. They are almost similar in shape and dimensions, but they differ in elastic and conductive properties. Mono-disperse gold colloids spread on an Au(1 1 1) substrate were imaged in ultra-pure water by TMAFM and by STM, and used as

reference sample. TMAFM characterization (images not included) showed single nano-particles with an apparent physical height very close to the nominal value of 5 nm. The STM measurements were performed at a tunnelling resistance of $4 \times 10^9\,\Omega$ (50 pA, 0.2 V) corresponding to a tunnelling distance of about 3 nm (Fig. 4). The corresponding height profile shows that the tip was retracted by about 5 nm when it was moved over the colloid. Therefore, the height of the metallic conductive bead measured by STM coincides with its physical height.

The situation appears different when PCSS molecules adsorbed on a gold substrate are imaged at the same tunnelling resistance ($4 \times 10^9\,\Omega$). Actually when the tip moves over the biomolecule a maximum tip retraction of 0.5 nm is registered (Fig. 5(a)). This value is significantly lower than the physical height of the protein (around 3 nm [52]). A reduced apparent height is a quite common feature displayed by biomolecules when imaged by STM [12,19,20,22–25], and might be attributed to their poorer conductivity as compared to the metallic substrate. However, the lateral size is well reproduced in agreement with the crystallographic data [52] and also with that reported by several authors on different biological samples [12,20,23,24]. It should be remarked that since we engaged at a tip–substrate distance of about 3 nm, and by considering a tip retraction of 0.5 nm, it is evident that the tip has not come into contact with the protein molecule.

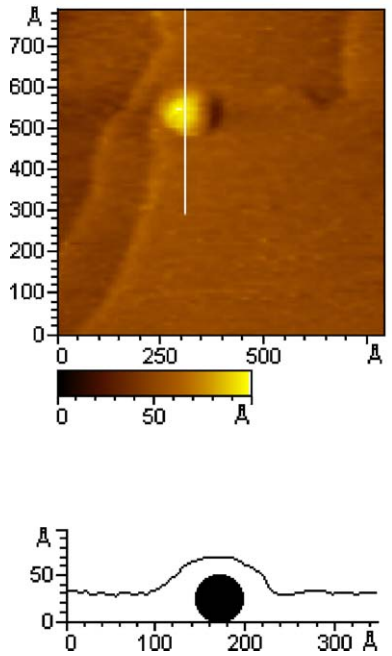

Fig. 4. Constant current STM image of a gold colloid on Au(1 1 1) surface at a tunnelling resistance of $4 \times 10^9\,\Omega$. Height profile along the vertical white line and sketch of the gold bead is shown below. Scan speed 4 Hz.

In other words, while the gold nano-particle can be imaged at any tunnelling resistance/distance, since the piezo can fully compensate for its presence, PCSS biomolecules can be imaged, in non-invasive way, only if the sum of the preset tip–substrate distance and the apparent height (corresponding to the maximum tip retraction over the biomolecule) exceed the topological height.

Taking into account the above-mentioned tip–substrate distance and the maximum tip retraction over the protein, we investigated the effect on the image quality upon lowering the gap by reducing the tunnelling resistance.

In the sequence of images shown in Fig. 5, PCSS molecules chemisorbed on an Au(1 1 1) substrate were imaged in ultra-pure water, at decreasing tip–substrate distances, which correspond to decreasing tunnelling resistances. When the tunnelling gap width was initially reduced from 2.9 to 2.4 nm no changes in shape or lateral dimensions were observed for the imaged proteins (Figs. 5(a and b)). In fact, here the tip can still overcome the height of the protein molecules, without interfering with their molecular structure.

However, when the initial tunnelling gap was reduced to 1.9 nm by setting the resistance to $4 \times 10^7\,\Omega$, some PCSS molecules display a considerable enlarged lateral dimension. For example, the molecule indicated by the white arrow increases its lateral size from 5.7 nm (Figs. 5(a and b)) to 14.9 nm (Fig. 5(c)). Finally, when the resistance is set to $2 \times 10^7\,\Omega$ (Fig. 5(d)), which corresponds to a tip–substrate distance of 1.4 nm, the lateral size of the indicated PCSS molecule was broadened to a value of 16.9 nm. In both Figs. 5(c and d), the tunnelling distance results below the physical

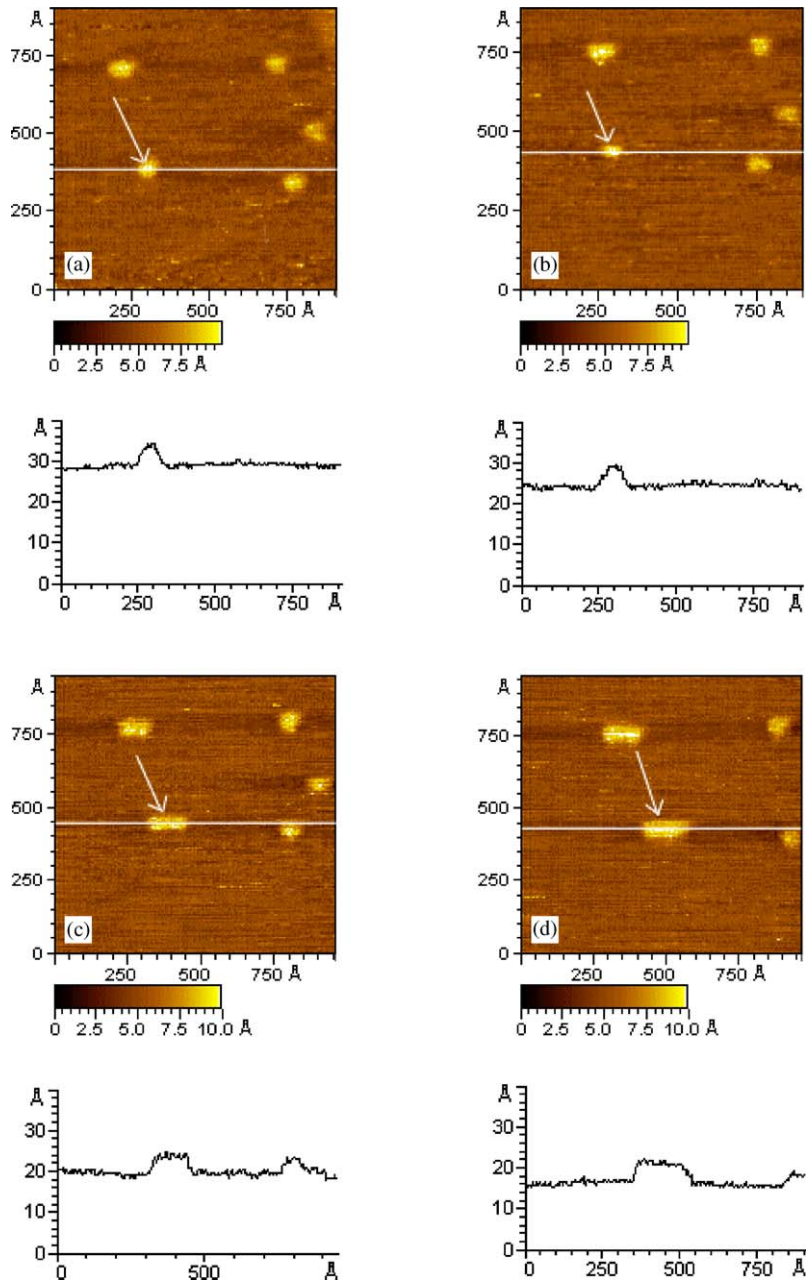

Fig. 5. PCSS molecules bonded on an Au(1 1 1) substrate as imaged by constant current STM in ultra-pure water at decreasing tunnelling resistances: $4 \times 10^9\,\Omega$ (a), $4 \times 10^8\,\Omega$ (b), $4 \times 10^7\,\Omega$ (c), $2 \times 10^7\,\Omega$ (d). Corresponding height profiles along white lines are shown below each figure. Scan speed 4 Hz. Vertical distances have been rescaled so that the height profiles coincide with the absolute tip position with respect to the substrate, as inferred by the *R–s* curve.

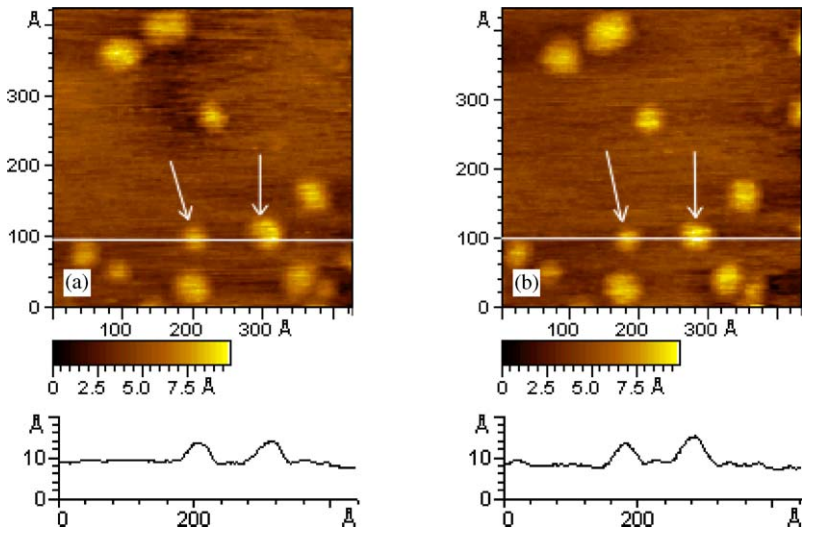

Fig. 6. Constant current STM images of PCSS proteins on a gold substrate in ambient atmosphere, at decreasing tunnelling resistances: $4 \times 10^9\,\Omega$ (a), $4 \times 10^6\,\Omega$ (b). Corresponding height profiles along white lines are shown below each figure. Scan speed 4 Hz.

height of the proteins. Therefore, even if the tip is still able to retract 0.5 nm over the protein, can either squeeze or pass through the protein, leading to invasive measurements of the biological sample. As a consequence, both lateral forces and vertical pressure may reasonably cause a deformation of the protein. In turn, the image will be a convolution of tip and sample, resulting in final enlarging of lateral dimensions. The strong interaction locally applied could affect either the structure or the function of the biomolecule, preventing any investigation of the inner electron transport properties. It has to be pointed out that not all the imaged molecules (Figs. 5(c and d)) are affected in the same way. This is consistent with the fact that the PCSS molecules may be oriented with respect to the gold substrate with different angles, yielding to a distribution of molecular heights centered on a mean value of 2.4 ± 0.6 nm [25,53].

In conclusion, the optimal image conditions for soft matter, which prevent one from observing artefact, are fulfilled when the sum of the tip–substrate distance and the tip retraction exceeds the physical height of the molecules.

For completeness, the sequential imaging of PCSS proteins was repeated in air, at tunnelling resistances similar to those used in the previous experiment. Images shown in Fig. 6 were recorded at $4 \times 10^9\,\Omega$ (a) and $4 \times 10^6\,\Omega$ (b), where the last one is close to the minimum operative tunnelling resistance for our instrument. According to the resistance–distance plot obtained in air, the corresponding tunnelling distances are now higher than those estimated in ultra-pure water. As estimated by the resistance–distance plot, the tunnelling gap width was 6.2 nm in Fig. 6(a) and 3 nm in Fig. 6(b). This implies that the tip never touched the proteins and, correspondingly, both images in Fig. 6 show single biomolecules with well-defined shape. Moreover, as shown by the height profile analysis, the lateral size is almost constant, and in good agreement with the expected lateral dimension.

4. Conclusion

The actual tip to substrate distance during the imaging of gold substrate has been determined by measuring the resistance as a function of the tunnelling gap. When the tunnelling resistance is set to $4 \times 10^9\,\Omega$, and Pt–Ir tips are used, distances of about 3 and 6 nm are estimated in water and in air, respectively. These tunnelling gap values are further confirmed by the destructive sequential

approach of the tip toward the Au substrate which leads to the formation of a bump at the contact site. We show that the starting tip–substrate distance becomes relevant in determining a non-invasive imaging in the case of biomolecules chemisorbed on metal substrates. For this purpose, PCSS molecules immobilized on gold (1 1 1) were imaged at different tunnelling resistances. These images displayed molecules whose lateral dimensions are well reproduced until the tip–substrate distance, added to the amount of tip retraction on the molecule, has a value above the physical vertical size of the protein, while molecule deformation and artefacts seem to appear as soon as the tunnelling distances are far below physical vertical size of the protein.

These results represent the first clear evidence of the crucial role of STM parameters to perform real non-invasive measurements on biomolecules. Results suggest that any time STM imaging on biomolecules has to be performed, the resistance–-distance dependence must be evaluated to establish the minimum tunnelling resistance at which the tip to substrate distance is at least equal, or even higher, the crystallographic dimension of the biomolecule; of course compatibly with an acceptable signal to noise ratio.

Further investigations are currently in progress to evaluate the impact of such a parameter on current transport mechanisms through/around biomolecules as obtained by STS.

Acknowledgments

This work has been partially supported by the FIRB-MIUR Project "Molecular Nanodevices" and by the EC Project "SAMBA" (V Frame FET).

References

[1] O. Marti, M. Amrein (Eds.), STM and SFM in Biology, Academic press Inc., San Diego, CA, 1993.
[2] A. Engel, Annu. Rev. Biophys. Chem. 20 (1991) 79 and references therein.
[3] R. Mukhopadhyay, Curr. Sci. 84 (2003) 1202 and references therein.
[4] R. Sonnenfeld, P.K. Hansma, Science 232 (1986) 211.
[5] S.M. Lindsay, T. Thundat, L. Nagahara, U. Knipping, R.L. Rill, Science 244 (1989) 1063.
[6] H.Y. Liu, F. Fan, C.W. Lin, A. Bard, J. Am. Chem. Soc. 108 (1986) 3838;
P. Lustenberger, H. Rohrer, R. Christoph, H. Siegenthaler, J. Electroanal. Chem. 243 (1988) 225;
K. Itaya, E. Tomita, Surf. Sci. 201 (1988) L507.
[7] J. Zhang, Q. Chi, A.M. Kuznetsov, A.G. Hansen, H. Wackerbarth, H.E.M. Christensen, J.E.T. Andersen, J. Ulstrup, J. Phys. Chem. B 106 (2002) 1131.
[8] J. Zhang, Q. Chi, S. Dong, E. Wang, Bioelectrochem. Bioener. 39 (1996) 267.
[9] A. Aviram (Ed.), Molecular Electronics-Science and Technology, AIP, New York, 1992.
[10] G. Leanna, D. Cyr, K. Muyskens, G.W. Flynn, Langmuir 14 (1998) 1465.
[11] S.J. Sowerby, M. Edelwirth, M. Reiter, W.M. Heckl, Langmuir 14 (1998) 5195.
[12] S.A. Contera, H. Iwasaki, Ultramicroscopy 91 (2002) 231.
[13] W. Han, E.N. Durantini, T.A. Moore, A.L. Moore, D. Gust, P. Rez, G. Leatherman, G.R. Seely, N. Tao, S.M. Lindsay, J. Phys. Chem. B 101 (1997) 10719;
S.M. Lindsay, O.F. Sankey, Y. Li, C. Herbst, A. Rupprecht, J. Phys. Chem. 94 (1990) 4655.
[14] M. Heim, R. Steigerwald, R. Guckenberger, J. Struc. Biol. 119 (1997) 212.
[15] F. Fan, A.J. Bard, Proc. Natl. Acad. Sci. USA 96 (1999) 14222.
[16] S.L. Tang, A.J. McGhie, Langmuir 12 (1996) 1088.
[17] E.P. Friis, J.E.T. Andersen, Yu.I. Kharkats, A.M. Kuznetsov, R.J. Nicols, J. Zhang, J. Ulstrup, atl. Acad. Sci. USA (1999) 1379.
[18] W. Schmickler, N.J. Tao, Electrochim. Acta 42 (1997) 2809.
[19] P. Facci, D. Alliata, S. Cannistraro, Ultramicroscopy 89 (2001) 291.
[20] J.J. Davis, H.A.O. Hill, Chem. Commun. 5 (2002) 393.
[21] J.J. Davis, Philos. Trans. R. Soc. 361 (2003) 2807.
[22] D.B. Kell, Bioelectrochem. Bioenergy 27 (1992) 235.
[23] J.J. Davis, C.M. Halliwell, H.A.O. Hill, G.W. Canters, M.C. van Amsterdam, M. Ph. Verbeet, New J. Chem. (1998) 1119.
[24] Q. Chi, J. Zhang, J.U. Nielsen, E.P. Friis, I. Chorkendorff, G.W. Canters, J.E.T. Andersen, J. Ulstrup, J. Am. Chem. Soc. 122 (2000) 4047.
[25] L. Andolfi, B. Bonanni, G.W. Canters, M.Ph. Verbeet, S. Cannistraro, Surf. Sci. 530 (2003) 18.
[26] Y. Selzer, A. Salomon, D. Cahen, J. Phys. Chem. B 106 (2002) 10432.
[27] X. Cui, A. Primak, X. Zarate, J. Tomfohr, O.F. Sankey, A.L. Moore, T.A. Moore, D. Gust, G. Harris, S.M. Lindsay, Science 294 (2001) 571.
[28] S.N. Yaliraki, M. Kemp, M. Ratner, J. Am. Chem. Soc. 121 (1999) 3428.
[29] J. Zhang, A.M. Kuznetsov, J. Ulstrup, J. Electroanal. Chem. 541 (2003) 133.
[30] W. Schmickler, J. Electroanal. Chem. 296 (1990) 283.

[31] L. Andolfi, M. Ph Verbeet, G. Canters, S. Cannistraro, Biophys. Chem. 107 (2004) 107.
[32] G.B. Khomutov, L.V. Belovolova, S.P. Gubin, V.V. Khanin, A.Yu. Obydenov, A.N. Sergeev-Cherenkov, E.S. Soldatov, A.S. Trifonov, Bioelectrochemistry 55 (2002) 177.
[33] P.B. Lukins, T. Oates, Biochim. Biophys. Acta 1409 (1998) 1.
[34] A. Vaught, T.W. Jing, S.M. Lindsay, Chem. Phys. Lett. 236 (1995) 306.
[35] J.R. Hahn, Y.A. Hong, H. Kang, Appl. Phys. A 66 (1998) S467.
[36] J.K. Gimzewski, R. Möller, Phys. Rev. B 36 (1987) 1284.
[37] G. Binnig, N. Garcia, H. Rohrer, J.M. Soler, F. Flores, Phys. Rev. B 30 (1984) 4816.
[38] R. Wiesendanger, H.-J. Güntherodt (Eds.), Scanning Tunneling Microscopy III, Springer, Berlin, 1995.
[39] N.D. Lang, Phys. Rev. B 52 (1995) 5335.
[40] M. Binggeli, D. Carnal, R. Nyffenegger, H. Siegenthaler, R. Christoph, H. Rohrer, J. Vac. Sci. Technol. B 9 (1991) 1985.
[41] W. Schmickler, D. Henderson, J. Electroanal. Chem. 290 (1990) 283.
[42] R. Christoph, H. Siegenthaler, H. Rohrer, H. Wiese, Electrochim. Acta 34 (1989) 1011.
[43] S.C. Meepagala, F. Real, Phys. Rev. B 49 (1994) 10761.
[44] Y.A. Hong, J.R. Hahn, H. Kang, J. Chem. Phys. 108 (1998) 4367.
[45] V. Guenebaut, M. Maaloum, M. Bonhivers, R. Wepf, K. Leonard, J.K.H. Hoerber, Ultramicroscopy 69 (1997) 129.
[46] M. Heim, R. Eschrich, A. Hillebrand, H.F. Knapp, R. Guckenberger, J. Vac. Sci. Technol. B 14 (1996) 1498.
[47] M.R. Redinbo, T.O. Yeates, S. Merchant, J. Bioenergy Biomembr. 26 (1994) 49.
[48] L. Andolfi, S. Cannistraro, G.W. Canters, P. Facci, A.G. Ficca, I.M.C. van Amsterdam, M. Ph. Verbeet, Arch. Biochem. Biophys. 399 (2002) 81.
[49] U. Dürig, O. Züger, IBM Res. Rep. RZ (1989) 1879.
[50] R.E. Thomson, J. Moreland, A. Roshko, Nanotechnology 5 (1994) 57.
[51] D.H. Huang, T. Nakayama, M. Aono, Appl. Phys. Lett. 73 (1998) 3360.
[52] M. Milani, L. Andolfi, S. Cannistraro, M. Ph. Verbeet, M. Bolognesi, Acta Crystallogr. D 57 (2001) 1735.
[53] A.R. Bizzarri, B. Bonanni, G. Constantini, S. Cannistraro, Chem. Phys. Chem. 4 (2003) 189.